Laser MBE-grown CoFeB epitaxial layers on MgO: Surface morphology, crystal structure, and magnetic properties

Andrey K. Kaveev,[1] Viktor E. Bursian,[1] Boris B. Krichevtsov,[1] Konstantin V. Mashkov,[1] Sergey M. Suturin,[1] Mikhail P. Volkov,[1] Masao Tabuchi,[2] and Nikolai S. Sokolov[1]

[1]*Ioffe Institute of Russian Academy of Sciences, St. Petersburg 194021, Russia*

[2]*Synchrotron Radiation Research Center, Nagoya University, Furo-cho, Chikusa, Nagoya 464-8603, Japan*

(Received 23 June 2017; revised manuscript received 20 September 2017; published 18 January 2018)

Epitaxial layers of CoFeB were grown on MgO by means of laser molecular beam epitaxy using $Co_{40}Fe_{40}B_{20}$ target. The growth was combined with *in situ* structural characterization by three-dimensional reciprocal space mapping obtained from reflection high energy electron diffraction (RHEED) data. High-temperature single stage growth regime was adopted to fabricate CoFeB layers. As confirmed by the atomic force microscopy, the surface of CoFeB layers consists of closely spaced nanometer sized islands with dimensions dependent on the growth temperature. As shown by RHEED and XRD analysis, the CoFeB layers grown at high-temperature on MgO(001) possess body centered cubic (bcc) crystal structure with the lattice constant $a = 2.87$ Å close to that of the $Co_{75}Fe_{25}$ alloy. It was further shown that following the same high-temperature growth technique the MgO/CoFeB/MgO(001) heterostructures can be fabricated with top and bottom MgO layers of the same crystallographic orientation. The CoFeB layers were also grown on the GaN(0001) substrates using MgO(111) as a buffer layer. In this case, the CoFeB layers crystallize in bcc crystal structure with the (111) axis perpendicular to the substrate surface. The magnetic properties of the CoFeB/MgO (001) heterostructures have been investigated by measuring magnetization curves with a vibrating sample magnetometer as well as by performing magneto-optical Kerr effect (MOKE) and ferromagnetic resonance (FMR) studies. FMR spectra were obtained for the variety of the magnetic field directions and typically consisted of a single relatively narrow resonance line. The magnetization orientations and the resonance conditions were calculated in the framework of a standard magnetic energy minimization procedure involving a single K_{1c} cubic term for the magnetocrystalline anisotropy. This allows a fairly accurate description of the angular dependences of the resonance fields—both in-plane and out-of-plane. It was shown that CoFeB layers exhibit in-plane fourth-order magnetic anisotropy. A two-step magnetization reversal model has been adopted for the CoFeB layers based on the VSM measurement analysis. Magnetization reversal studies performed by polar MOKE indicate that the magnetization lies in-plane in absence of magnetic field. Observed magnetic field dependences of reflected light ellipticity in geometry of longitudinal Kerr effect give convincing evidence for contribution of quadratic in magnetization terms in the dielectric tensor and clearly show the in-plane magnetization rotation.

DOI: 10.1103/PhysRevMaterials.2.014411

I. INTRODUCTION

The existing interest to the thin layers of magnetic metallic alloys is related to various potential applications of these materials in spintronics, magnonics, etc. Especially attractive among those are three-component three-dimensional (3D) metallic and Heusler alloys because of high degree of spin polarization [1,2]. These alloys are perspective for application in novel mass storage devices, such as magnetic tunnel junction (MTJ)-based magnetic random access memory (MRAM) [3], allowing high-density and extended-time stability information storage, and spin injection devices [4,5]. The fundamental interest to investigate magnetization behavior in thin CoFeB ferromagnetic films is motivated by (i) low-spin wave damping [6] (in comparison with other metallic systems) that is important for developing spintronic transmitting devices based on CoFeB layers integrated into monolithic integrated circuits; (ii) the possibility to tune magnetization orientation by external electric field or by substrate-induced layer deformations [7,8], exploring the sensitivity of surface anisotropy in CoFeB thin films to the electric field; (iii) interesting proximity effects (such as exchange bias, induction of atypical magnetic order, etc.) in CoFeB based FM/FM and FM/AFM (i.e., antiferromagnetic) systems [9,10].

It is known that admixing boron to the CoFe system allows decreasing the coercivity and FMR resonance line width as well as flattening the interface [11,12]. Some authors have mentioned a disorder related to boron oxide formation at the CoFeB/MgO interface [13] and distortion in Δ_1 state symmetry caused by boron atoms presence which in turn tempers majority channel conductance [14]. Thus, boron influence on the CoFeB thin films physical properties is not yet clearly understood and should be thoroughly studied.

The majority of recent studies deals with MTJs fabricated in the form of CoFeB/MgO/CoFeB trilayers that are grown at room temperature (RT) and subjected to post-growth high-temperature annealing. It is known that the large TMR value related to the symmetry filtering effect [15] is observed in MgO with (001) surface orientation, while the epitaxial metallic films (acting as metallic contacts in MTJs) usually grow

with (111) surface orientation. The (111) → (001) orientation reversal in Me/CoFeB/MgO/CoFeB/Me systems fabricated for MTJ applications is usually achieved through annealing CoFeB grown at RT. As a consequence of the RT growth the crystal quality of CoFeB and MgO layers fabricated in this way is usually not perfect—e.g., MgO layers become (001)-textured instead of being monocrystalline [16]. The present work aims at improving the crystal quality of the CoFeB(001)/MgO(001)/CoFeB(001) MTJ system and is motivated by the fact that the higher crystalline quality is known to enhance the TMR effect [17]. For this purpose, the specific technology of MBE growth was developed and used for fabrication of CoFeB layers on MgO(001) and MgO/GaN(0001) substrates.

The paper is organized as follows. In Sec. II the experimental aspects of preparation, surface morphology characterization, investigation of crystal structure, and magnetic properties of CoFeB layers are presented. Results of structural characterization are given in Sec. III; Sec. IV is devoted to the static and dynamic magnetic properties of the fabricated nanostructures; Sec. V gives the summary of the studies performed.

II. EXPERIMENTAL

CoFeB/MgO(001) and CoFeB/MgO(111)/GaN(0001) layers were grown using a "Surface GmbH" laser MBE system equipped with KrF excimer laser used to ablate CoFeB and MgO targets. To dehydrate and smoothen the MgO(001) surface the substrates were annealed to 650 °C for 30 min in oxygen or argon atmosphere at a pressure of 1.5×10^{-3} mbar. To further improve the surface quality a 5–15 nm MgO buffer layer was deposited at 500 °C on top of the MgO(001) substrate. In contrast to the majority of works where MgO is grown via magnetron sputtering with use of pure Mg target in oxygen atmosphere, the possibility to grow MgO from MgO stoichiometric target in Ar atmosphere was demonstrated. Taking into account that CoFeB growth is only possible in a nonoxidizing argon atmosphere, using argon instead of oxygen also for the MgO growth gives the advantage of a single gas technology. Before MgO growth GaN(0001) substrates were annealed at 300 °C. The deposition of 5–10 nm thick MgO buffer layer on GaN was performed at 450 °C in 1.5×10^{-3} mbar of oxygen.

The CoFeB growth was performed with use of $Co_{40}Fe_{40}B_{20}$ target in argon at a pressure of 2.5×10^{-3} mbar. Typical deposition rate was about $0.03 - 0.07$ Å s^{-1}. Most of the samples were grown below 500 °C to avoid undesirable boron migration to the interfaces, which was observed earlier during high temperature annealing [13]. While the boron presence in the studied samples was confirmed by Auger electron spectroscopy measurements, the boron concentration profiles were not studied in the samples grown at high temperature. Preliminary Auger electron spectroscopy and XPS measurements enabled evaluation of boron concentration in the films as 5–10 at. %. The percentage of boron is appeared to be less than 20 at. % as by some kinetic effects during the ablation (a part of boron atoms from the target doesn't arrive to the substrate), so by the migration of boron to the interfaces and subsequent oxidation and flying out. Not so high boron concentration likely promoted the CoFeB epitaxial growth in our experiment.

In situ reciprocal space 3D mapping by high-energy electron diffraction (RHEED) and x-ray diffraction (XRD) was carried out with the use of the dedicated software developed by the authors [18,19]. Three-dimensional reciprocal space maps were built from dense sequences of two-dimensional diffraction patterns obtained during sample rotation around the surface normal. Three-dimensional mapping approach allows building and visualization of arbitrary reciprocal space projections and cross sections as well as performing comparison to the calculated reciprocal lattice models. An important feature of the applied RHEED 3D mapping technique is the possibility to obtain the "plan-view" reciprocal space projections—the views of the reciprocal space seen along the surface normal. The plan-view available in RHEED only through the 3D mapping technique allows effective estimation of the in-plane symmetry, in-plane epitaxial relations, and the degree of in-plane crystalline order. X-ray diffraction measurements were performed *ex situ* at BL3A beamline of Photon Factory synchrotron (Tsukuba, Japan). The oscillation measurement in the x-ray reflectivity profiles provided convenient additional measure of the film thickness.

Atomic force microscopy (AFM) measurements were carried out using the ambient air NT-MDT microscope operating in the semicontact mode. Polar and longitudinal magneto-optical Kerr effects were measured at wavelengths of 633, 535, and 405 nm (for experiment geometry and parameters see Refs. [20,21]). Ferromagnetic resonance (FMR) measurements were carried out using an X-band EPR spectrometer. Magnetization curves were measured by the Quantum Design PPMS-9 system (Quantum Design Inc., San Diego, CA) at room temperature.

III. CoFeB/MgO SURFACE MORFOLOGY AND CRYSTAL STRUCTURE

In the previous works, the CoFeB layers were usually fabricated by using a two-step technology: an amorphous film was first grown at room temperature and then crystallized by high temperature annealing. In this case, the interface region of the CoFeB film gets textured consisting of grains oriented with [001] axis perpendicular to the film plane. The film regions located far from the interface consist of grains with arbitrary orientation of the crystal axes [22]. It is of interest to compare the surface morphology and crystal structure of the films fabricated by the conventional method mentioned above and by the advanced single stage high temperature technique adopted in the present work.

A. Surface morphology

The initial surface of the GaN substrate has the step-and-terrace morphology that is not modified on the micron scale when MgO buffer layer is deposited at 350 °C [Fig. 1(a)]. To get similar surface morphology on the MgO substrate [Fig. 1(b)] the latter is first annealed at 800 °C and then overgrown with MgO at 400−500 °C. The substantial flattening of the MgO surface is confirmed by evolution of the RHEED patterns from dots before [Fig. 1(c)] to streaks after [Fig. 1(d)] the overgrowth.

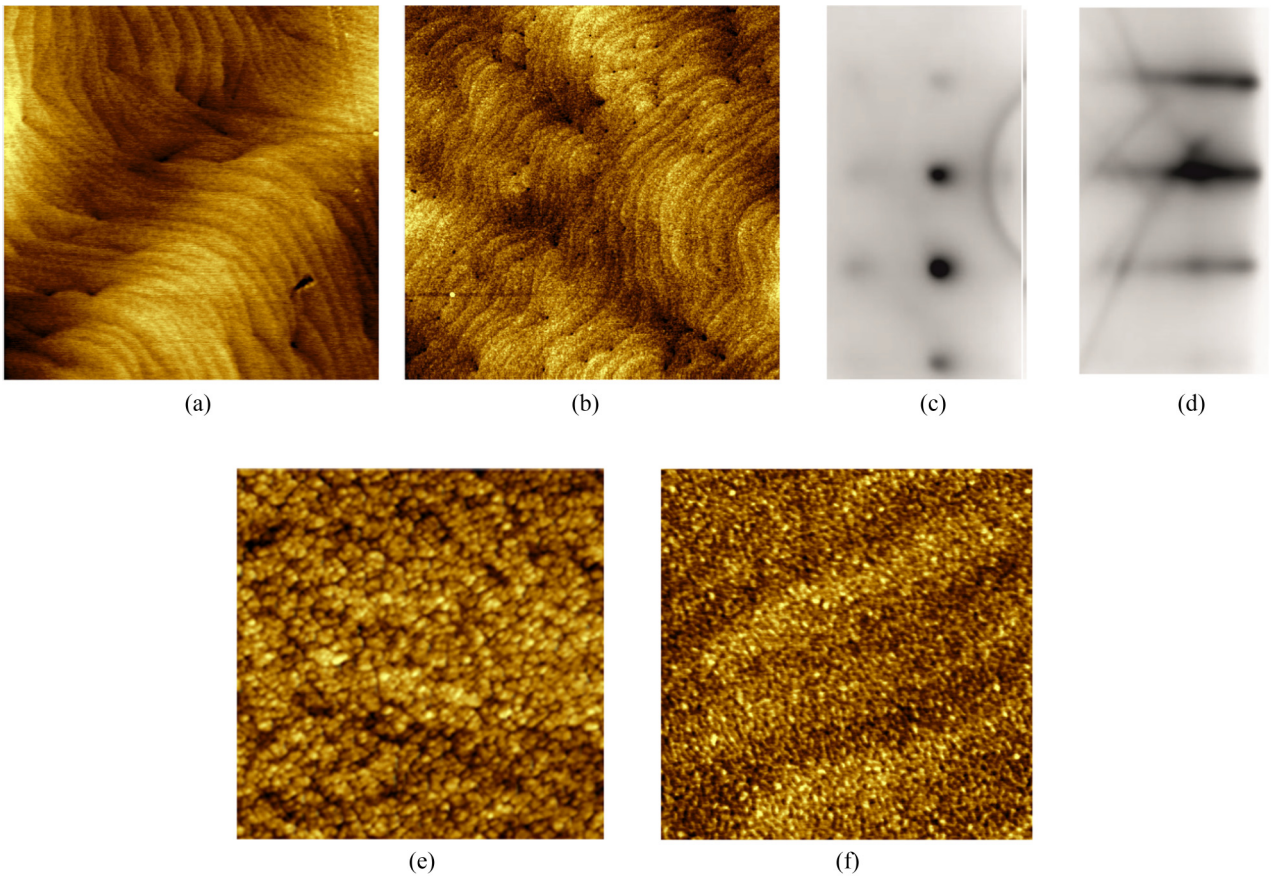

FIG. 1. Surface morphology of MgO buffer layer grown on MgO(001) ((3600 nm × 3600 nm × 16 nm, 150 °C) (a) and GaN(0001) (3500 nm × 3500 nm × 10 nm, 350 °C) (b). RHEED patterns of MgO(001) surface ([100 zone axis]) before (c) and after (d) MgO overgrowth. The surface morphology of 10-nm-thick CoFeB(001) films grown on MgO(001)/MgO(001) (e) and MgO(111)/GaN (0001) at 500 °C (f). AFM image size 660 × 660 × 4 nm.

The surface morphologies of the CoFeB layers grown on MgO(001)/MgO(001) at 700 °C and on MgO(111)/GaN(0001) at 500 °C are shown in Figs. 1(e) and 1(f). Dense arrays of CoFeB islands are present at the surface in both cases.

B. Crystal structure of CoFeB layers

Crystal structure of the CoFeB layers was studied by 3D reciprocal space mapping using *in situ* electron (RHEED) and *ex situ* x-ray diffractometry.

1. CoFeB/MgO(001)

As the electron diffraction at grazing incidence is only sensitive to the near-surface region, the substrate and the film can be studied separately by RHEED. RHEED maps of the MgO substrate and of the CoFeB layer are shown in the upper part of Fig. 2. The maps on the left show the reciprocal space cross-sections containing a single reciprocal space zone—with the [1–10] zone axis for MgO and the [010] zone axis for CoFeB. The maps on the right show the plan-view reciprocal space projections with the projection line parallel to the surface normal. The observed RHEED patterns show distinct transmission spots combined with weak streaks at low q_z (out-of-plane momentum transfer component) in agreement with the moderate surface roughness observed by AFM. The results of reciprocal lattice modeling are superimposed on the maps in Fig. 2 allowing us to conclude that CoFeB grows epitaxially with the body centered cubic (bcc) crystal structure oriented with its [001] axis perpendicular to the surface. Obtained from the modeling $a \approx 2.87$ Å lattice constant of CoFeB is close to that of obtained from θ to 2θ XRD curves (not shown here) $a = 2.88$ Å. Both of them are slightly larger than $a = 2.842$ Å of $Co_{75}Fe_{25}$ [23]. This increase can be attributed to presence of interstitial boron atoms in the film. The in-plane CoFeB [010] axis is oriented along the MgO [110] axis favored by the fact that MgO lattice constant is approximately $\sqrt{2}$ times larger than that of CoFeB.

In contrast to RHEED, x-ray diffraction allows probing the crystal structure deep below the surface. In the XRD maps one can simultaneously observe reflections from every component of the heterostructure including the substrate. This is convenient for accurate estimation of epitaxial relations and lattice constants. In addition XRD is sensitive to any kind of the post growth crystal structure modification. In the present case, the epitaxial relations in the CoFeB/MgO (001) system revealed earlier by RHEED were confirmed by x-ray diffraction measurements. Figure 2 shows reciprocal space projection XRD maps built perpendicular and parallel to the sample surface. The projection axes are the same as in the RHEED maps discussed above. When comparing RHEED and

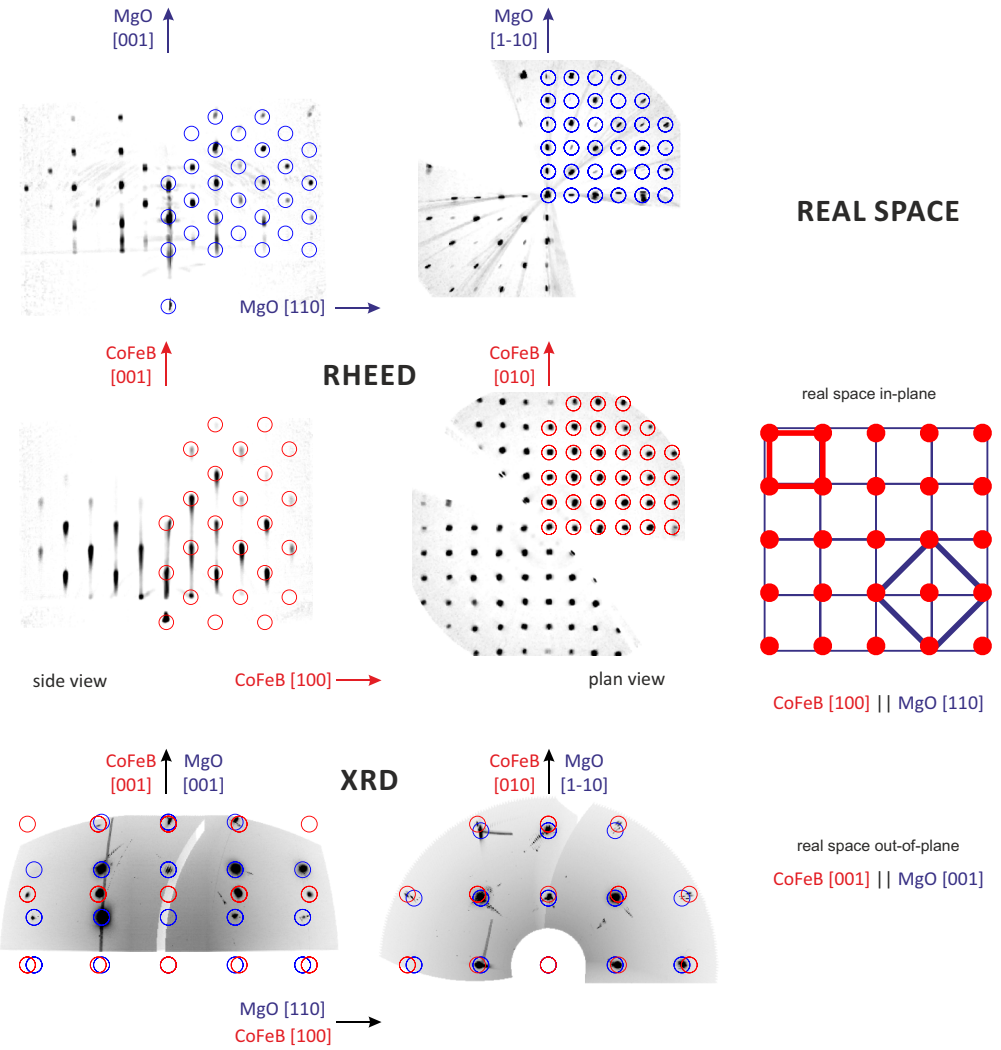

FIG. 2. RHEED (surface) and XRD (bulk) reciprocal space maps of CoFeB(001) layer and MgO(001) substrate with superimposed model reflections. Schematic presentation of CoFeB(001)/MgO(001) in-plane lattice matching is shown on the right.

XRD maps one has to take into account the different scales (XRD is three times zoomed in) and the fact that RHEED side views are reciprocal space cross-sections while XRD side views are reciprocal space projections. The lattice constant of CoFeB was estimated as 2.87 ± 0.02 Å by analyzing the XRD intensity profiles.

Unexpectedly, the RHEED maps obtained during CoFeB growth on MgO(001) (and on GaAs(001) discussed elsewhere [24] show a nontrivial $[\sqrt{2} \times \sqrt{2}]$ R45 superstructure in case of optimized growth conditions, especially very smooth MgO surface. This superstructure marked with blue rectangles in the RHEED maps appears as half order streaks on the reciprocal space cross section perpendicular to CoFeB [1–10] [Fig. 3(a)] and square centering dots on the reciprocal space projection along the CoFeB [001] normal [Fig. 3(b)].

The possible explanation of this superstructure is shown in Fig. 3(c). Taking into account that CoFeB has bcc crystalline structure formed by alternating metallic planes (as a possibility, of alternating Co and Fe [25]) in [001] direction, we suppose that such superstructure may be formed by half-filled top metal plane (solid and open dark (violet online) circles). This explanation seems to be quite simple and understandable but other models (related for example to chemical ordering of the Co and Fe, etc.) are not excluded.

It was revealed that using the high temperature growth approach it is also possible to grow the top epitaxial MgO layer required in the MgO/CoFeB/MgO MTJ heterostructures. An important finding is that though the top MgO layer is not in direct contact with the bottom MgO layer, both show the same crystallographic orientation. This opens a way to fabricate high structural quality [MgO/CoFeB $\times N$] superlattices, which could have unusual magnetic properties [26,27].

2. CoFeB/MgO(111)/GaN(0001)

The (001) orientation of substrate is widely used in magnetic tunnel junction devices. There is only limited information on CoFeB layers grown on substrates of other orientations. Among them CoFeB (111) orientation looks quite attractive because of recent interest to GaN(0001)-based heterostructures.

Unexpected epitaxial relations were observed for the CoFeB layer epitaxially grown on MgO/GaN(0001). As expected, the

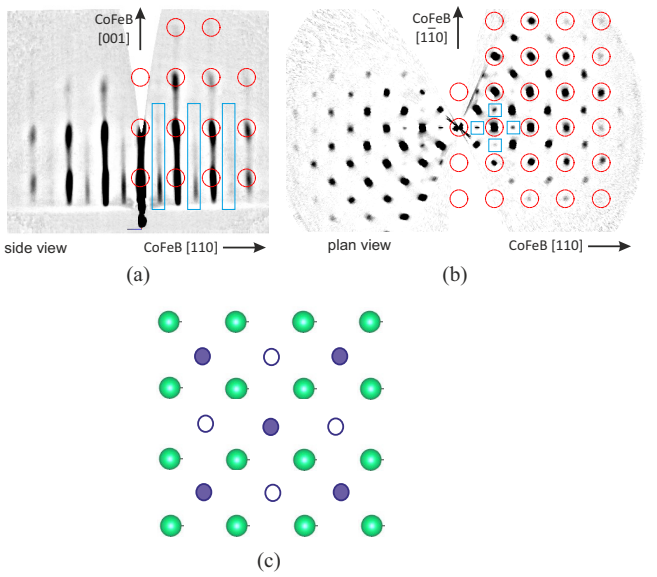

FIG. 3. RHEED reciprocal space maps showing $\sqrt{2} \times \sqrt{2}$ R45 superstructure in CoFeB/MgO (001) layer: side view cross-section perpendicular to CoFeB [1–10] (a) and projection along CoFeB [001]. (b). Superimposed on the maps are the modeled CoFeB reflections (circles, red online) and the superstructure features (rectangles, blue online). (c) The possible explanation of this superstructure. Green circles are related to the bottom Me layer, filled (blue online) circles—to the half-filled top Me layer, empty blue circles—empty metal positions of the top layer.

MgO buffer layer on GaN shows well-established epitaxial relations : MgO (111) ‖ GaN (0001), MgO [1–10] ‖ GaN [11–20] in agreement with [28,29]. As can be seen in Fig. 4, the RHEED maps of CoFeB layer show quite complicated reflection pattern both on the side and plan views. The comparison of the patterns to model reciprocal lattices allowed us to ascribe the observed reflection pattern to CoFeB lattice oriented with the [110] axis perpendicular to the surface. Due to the C_{3v} symmetry of the underlying MgO(111) surface there exists three equally probable CoFeB lattices rotated by 120° around the surface normal with respect to each other. Comparing the MgO and CoFeB plan view reciprocal space projections shown in Fig. 4, one can describe the in-plane epitaxial relations as follows: CoFeB [001] ‖ MgO⟨−110⟩. This quite unusual CoFeB layer lattice orientation is likely related to the reasonable matching between the MgO surface periodicity along the [110] direction ($a_{MgO}/\sqrt{2} = 4.212$ Å$/\sqrt{2} = 2.98$ Å) and the CoFeB periodicity along the [100] direction ($a = 2.87$ Å). In the perpendicular direction, three CoFeB rows roughly match two MgO rows (see the sketch in Fig. 4). Measurements of magnetic properties of such films are in progress and will be published elsewhere.

IV. MAGNETIC PRORERTIES OF CoFeB/MgO(001) HETEROSTRUCTURES

The magnetic properties were studied at room temperature by measuring magnetization curves with vibrating sample magnetometer (VSM), by studying ferromagnetic resonance (FMR), polar magneto-optical Kerr effect (PMOKE) and longitudinal magneto-optical Kerr effect (LMOKE). The experimental data presented below refer to the typical 20 nm CoFeB/MgO sample grown at 400 °C. The data were analyzed within a conventional theory and fitted with a single set of magnetic parameters. Other samples with the same thickness and growth conditions show qualitatively same results with slightly different parameter values.

A. Ferromagnetic resonance

The FMR spectra and their angular dependences were measured at a fixed microwave frequency $\nu_0 = 9.33$ GHz, while the applied magnetic field **H** in a chosen direction was scanned by its magnitude H_0. Due to small (∼1 Oe) modulation of H_0 and the differential registration technique, the spectra show the absorption derivative dA/dH_0 versus H_0.

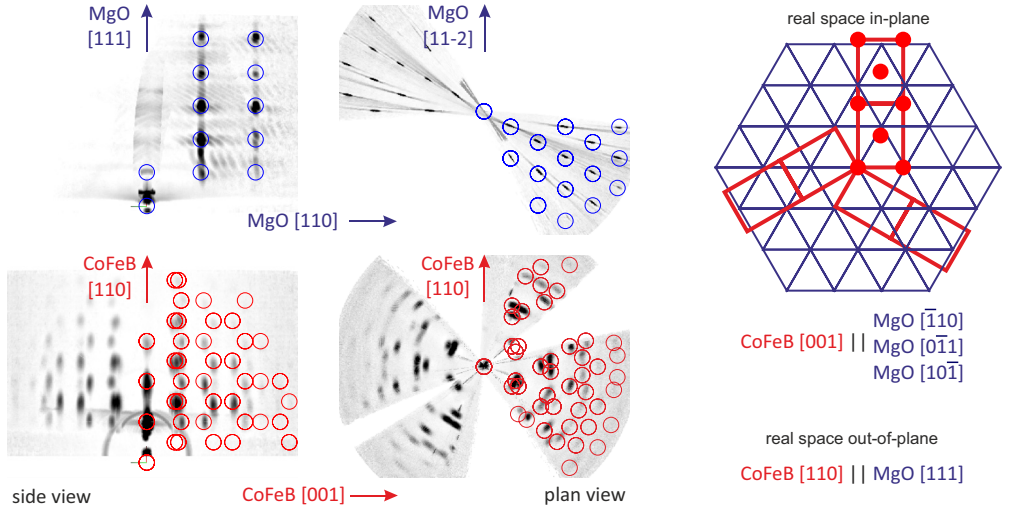

FIG. 4. RHEED reciprocal space maps of MgO (111) buffer layer grown on top of GaN (0001) and of CoFeB layer grown on top of MgO(111) buffer layer. Schematic presentation on the right shows CoFeB(110)/MgO(111) in-plane lattice matching.

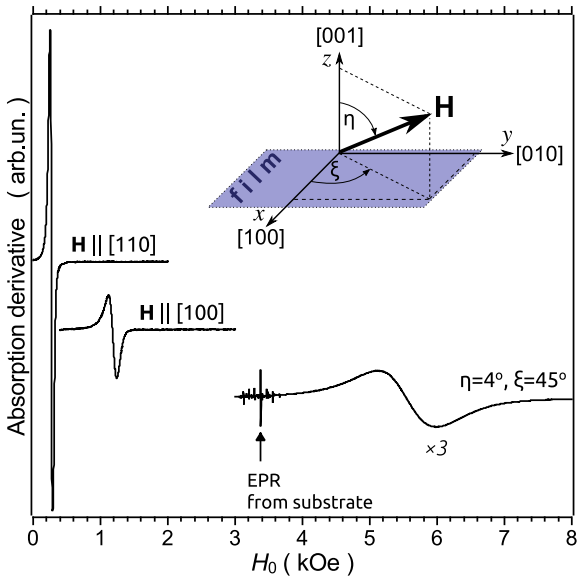

FIG. 5. FMR spectra taken at 9.33 GHz with three orientations of scanning magnetic field **H**: **H** ∥ [110], **H** ∥ [100], and **H** close to [001]. The latter spectrum is multiplied by factor 3. The inset defines polar (η) and azimuthal (ξ) angles of **H** in the crystallographic coordinate system of the CoFeB lattice (x,y,z).

It is seen (Fig. 5) that both the resonance field $H_{\rm res}$ and the line width ΔH strongly depend on the orientation of magnetic field relative to the CoFeB crystal axes. The narrowest line ($\Delta H = 35$ Oe) is observed when H lies in the plane of the film parallel to the [110] direction. Comparable values of ΔH have been observed in some CoFeB films [30,31].

The angular dependences of the resonance fields $H_{\rm res}$ (η,ξ) were measured (Figs. 6 and 7) in three planes, where one of the angles varies and the other remains constant. The in-plane angular dependence (Fig. 6) clearly manifests a *fourfold* symmetry, or, in other words, a *biaxial* magnetic anisotropy, without any admixture of in-plane uniaxial magnetic anisotropy. This is in contrast to CoFeB films obtained previously by annealing, where the in-plane uniaxial magnetic anisotropy has been observed [31].

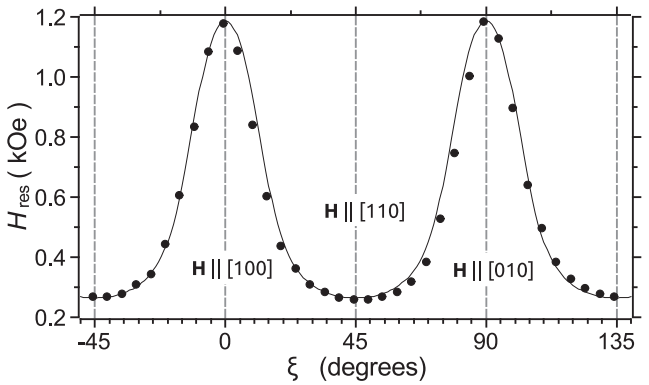

FIG. 6. In-plane ($\eta = 90^\circ$) FMR angular dependence of $H_{\rm res}$ (ξ): dots—experiment, solid line—calculations described below.

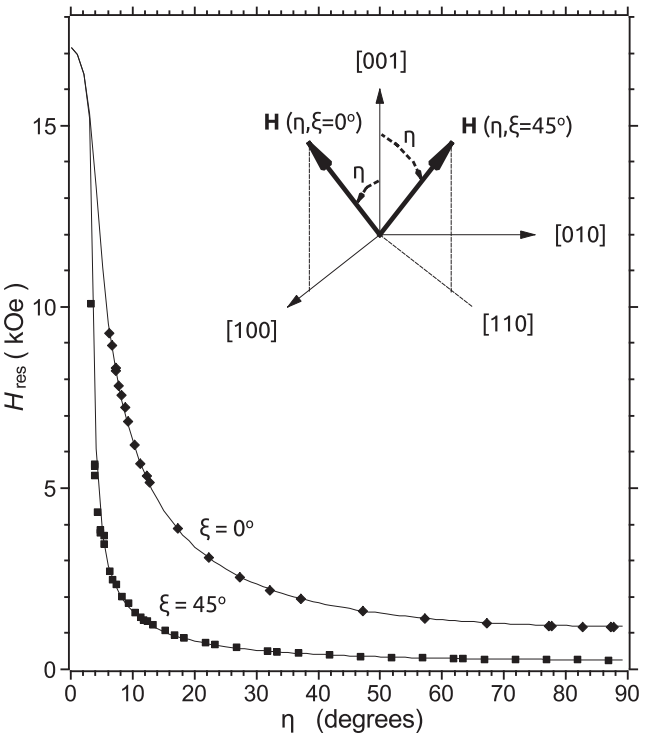

FIG. 7. Out-of-plane FMR angular dependences of $H_{\rm res}$ (η): diamond dots—$\xi = 0^\circ$ (H rotates from [001] to [100] in the (010) plane); square dots—$\xi = 45^\circ$ (H rotates from [001] to [110] in the (110) plane); solid lines—calculations.

To fit these experimental data, we take the magnetization energy density in the following form:

$$\varepsilon = -\vec{H}\vec{M} + \frac{4\pi M_z^2}{2} + \frac{K_{c1}}{M_s{}^4}\left(M_x^2M_y^2 + M_y^2M_z^2 + M_z^2M_x^2\right) - \frac{K_{u1}M_z^2}{M_s^2}, \quad (1)$$

where the four terms are: Zeeman energy, demagnetizing term due to sample form factor, cubic anisotropy term due to the CoFeB crystal structure, and uniaxial anisotropy in the direction normal to the film plane. The latter could be expected due to surface/interface magnetic anisotropy [32], which can arise in particular due to lattice mismatch between the CoFeB layer and the substrate or overlap between the O-p_z and transition metal dz^2 orbits [33]. Being the function of **H** and magnetization vector **M**, ε depends on three parameters: saturation magnetization M_s, cubic anisotropy constant K_{c1}, and uniaxial anisotropy constant K_{u1}. It can also be expressed in polar coordinates:

$$\varepsilon(\vartheta,\varphi,H_0,\eta,\xi) = -H_0M_s(\cos(\varphi-\xi)\sin\eta\sin\vartheta - \cos\eta\cos\vartheta) + \frac{K_{c1}}{4}(\sin^4\vartheta\sin^2 2\varphi + \sin^2 2\vartheta) + \left(2\pi M_s^2 - K_{u1}\right)\cos^2\vartheta, \quad (2)$$

where H_0 stands for the magnitude of **H**, η, and ξ—its polar and azimuth angles (as shown in the inset to Fig. 5), and analogously, θ and φ—the polar and azimuth angles of **M**. With η and ξ fixed within a certain experiment, the

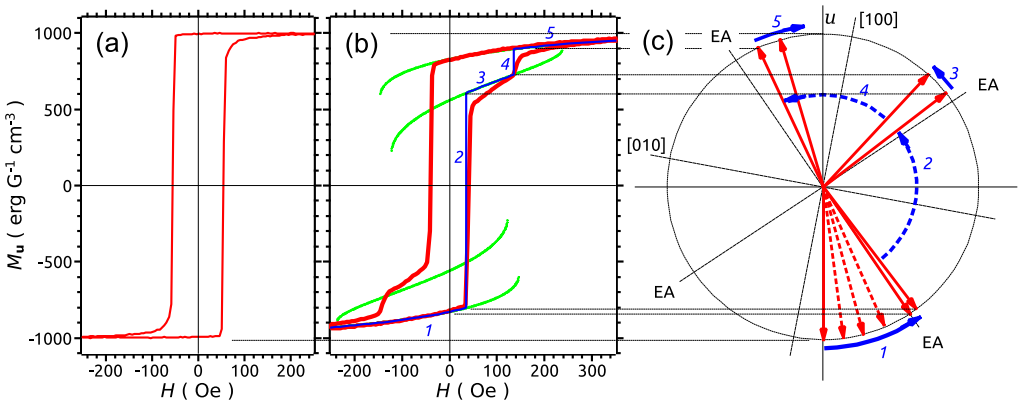

FIG. 8. Magnetization curves (red lines in the online version) measured by VSM with magnetic field **H** lying in the film plane. (a): $\xi = 45^\circ$, **H** ∥ [110] (easy axis); (b): $\xi \approx 11^\circ$. Green lines in part (b), different solutions for M_u (H), which is the projection of **M** onto **H** direction; blue line in part (b) shows our assumption on how the magnetization jumps from one solution to another; (c) scheme of magnetization rotation.

calculation procedure searches equilibrium angles θ and φ by minimization of $\varepsilon(\theta,\varphi)$. This gives stable (main minimum) or metastable (other minima) solutions for the direction of static magnetization, and the FMR field $H_{\rm res}$ can be found as a root of resonance equation:

$$\nu_0 = \frac{\gamma}{2\pi M_s \sin\theta}\sqrt{\frac{\partial^2\varepsilon}{\partial\varphi^2}\frac{\partial^2\varepsilon}{\partial\theta^2} - \left(\frac{\partial^2\varepsilon}{\partial\varphi\partial\theta}\right)^2}, \qquad (3)$$

where the gyromagnetic ratio $\gamma = g|e|/2m_e c$. The solid lines in Figs. 6 and 7 were calculated following the described procedure with numerical minimization at each H_0 and numerical root finding. Although the magnetic constants could be found by best fitting, in our case, there are simple analytical expressions binding these constants with the resonance fields H_{100}, H_{110}, and H_{001} for the directions [100], [110], and [001]:

$$\left(\frac{2\pi\nu_0}{\gamma}\right)^2 = (H_{100}+2k_{c1})(4\pi M_{\rm eff}+H_{100}+2k_{c1}),$$
$$\left(\frac{2\pi\nu_0}{\gamma}\right)^2 = (H_{110}-2k_{c1})(4\pi M_{\rm eff}+H_{110}+2k_{c1}),$$
$$\frac{2\pi\nu_0}{\gamma} = H_{001}-4\pi M_{\rm eff}+2k_{c1}, \qquad (4)$$

where the two renormalized parameters $4\pi M_{\rm eff} = 4\pi M_s - 2K_{u1}/M_s$ and $k_{c1} = K_{c1}/M_s$ have been used instead of the primary M_s, $K_{\rm c1}$, and $K_{\rm u1}$. It should be emphasized, that the Eqs. (4) are of a limited applicability, because they are valid only when ν_0 and therefore the resonance fields are large enough to align **M** ∥ **H**. As to the later condition, it has to be checked by a correct minimization procedure. On the other hand, if valid, they unambiguously bind all three magnetic parameters γ, $M_{\rm eff}$, and k_{c1} with three resonance fields at the extrema of FMR angular dependence that can be measured experimentally with high accuracy.

As the spectrometer limitations do not allow measuring above 10 kOe, we were unable to obtain H_{001}, which leaves only two equations for three parameters. However, taking $g = 2.1$ as a reasonable guess [34], the other two can be calculated from Eq. (4):

$$4\pi M_{\rm eff} = 13.5\,{\rm kG}, \quad k_{c1} = 0.24\,{\rm kG}. \qquad (5)$$

It is seen from Figs. 6 and 7 that, with these parameter values, the calculated FMR angular dependences are in good agreement with the experiment.

B. Vibration sample magnetometry

Magnetization curves measured by VSM with magnetic field **H** ∥ [110] in the film plane show square hysteresis loops [Fig. 8(a)] with abrupt magnetization jump taking place at $H_{\rm c} \approx \pm 50$ Oe. Such behavior is characteristic for magnetization switching related to nucleation of opposite domains and subsequent domain wall movement. The hysteresis loop shape changes, essentially, when **H** rotates in the film plane away from the easy axis [110]. Analogous to the FMR, the curves qualitatively repeat with 90° periodicity, and the most impressive is the appearance of antisymmetric "shoulders" [Fig. 8(b), *red line in the online version*] at the **H** directions close to [100] and [010].

Analysis of magnetic energy Eq. (2) shows that such shoulder may be attributed to a two-step magnetization reversal. The increase of magnetic field from large negative value $H \sim -300$ Oe to positive value $H \sim 40$ Oe is followed by magnetization rotation [line 1 in Figs. 8(b) and 8(c)]. At the first step the magnetization jump at $H \sim 40$ Oe corresponds to transition into metastable state [line 2 in Figs. 8(b) and 8(c)], which at this field has almost the same energy as the stable one. The jump goes through domain wall nucleation and movement and after the jump the magnetization orientation is approximately perpendicular to the one just before the jump [line 3 in Figs. 8(b) and 8(c)]. At $H \sim 120$ Oe the second jump takes place that corresponds to transition into the stable state (line 4). After the second jump, the increase of magnetic field results in magnetization rotation to the direction of magnetic field. On the opposite hysteresis loop branch the jumps take place at $H \sim -40$ Oe and $H \sim -120$ Oe, correspondingly. The theoretical curves in Fig. 8(b) were calculated with the following set of parameters:

$$4\pi M_s = 12.6\,{\rm kG}, \quad k_{c1} = 0.24\,{\rm kG}, \qquad (6)$$

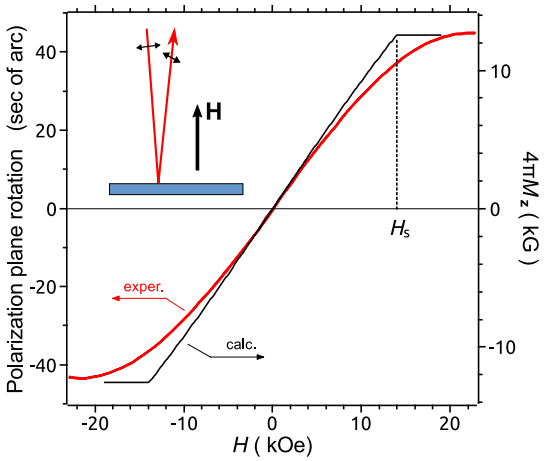

FIG. 9. Light polarization plane rotation due to polar Kerr effect in magnetic field $H \parallel [001]$ perpendicular to the film plane. Red line (in the online version) —experiment; black line—calculated with the parameter sets Eqs. (5) and (6) as being proportional to magnetization projection M_z.

where the value of k_{c1} is taken from FMR angular dependence (0.24 kG, see above), and the value of M_s—from the saturation magnetization in Fig. 9(a). The value of cubic magnetic anisotropy parameter can be now calculated: $K_{c1} = M_s\, k_{c1} = 2.4 \times 10^5\,\mathrm{erg\,cm^{-3}}$, which is close to that observed in $Fe_xCo_{1-x}(001)/ZnSe/GaAs$ epitaxial nanostructures [35]. The difference between $4\pi M_s$ and $4\pi M_{\mathrm{eff}}$ could reveal the presence of uniaxial anisotropy $2K_{u1}/M_s = 4\pi M_s - 4\pi M_{\mathrm{eff}} \approx -0.9\,\mathrm{kG}$, which is interface and/or surface related. On the other hand, it is relatively small (7%), differs from sample to sample and could result from possible errors in the film volume estimations. Note that analogous hysteresis loops were observed and interpreted recently in Fe/MgO(001) samples in Ref. [36].

C. Magneto-optical Kerr effect magnetometry

Magnetic field dependencies of PMOKE were measured at $\lambda = 530\,\mathrm{nm}$ in magnetic field oriented perpendicularly to the film plane. We subtracted the linear in H contribution of Faraday effect, which comes from the substrate and can be distinguished at $H > 20\,\mathrm{kOe}$. The PMOKE dependence is reversible, without any hysteresis (Fig. 9, red line). This indicates that in the absence of the magnetic field the magnetization **M** lies in the film plane and the out-of-plane magnetic field induces out-of-plane magnetization rotation. Magnetization curves measured by PMOKE are analogous to that obtained recently in CoFeB layers by means of VSM [30,37]. The saturation of magnetization in thin films should take place at $H_s = 4\pi M_s - H_a$, where $H_a = 2k_{c1} + 2k_{u1}$ is the anisotropy field, which can stimulate the in-plane ($H_a < 0$) or out-of-plane ($H_a > 0$) orientation of magnetization in addition to demagnetizing field $H_d = 4\pi M_s$, which stimulates the in-plane orientation of **M** due to the form factor. Ideally, the dependence should look like a broken line (Fig. 9, black line) with an abrupt fracture at H_s. Experimentally, the dependencies are essentially smoothed, which may be caused by small

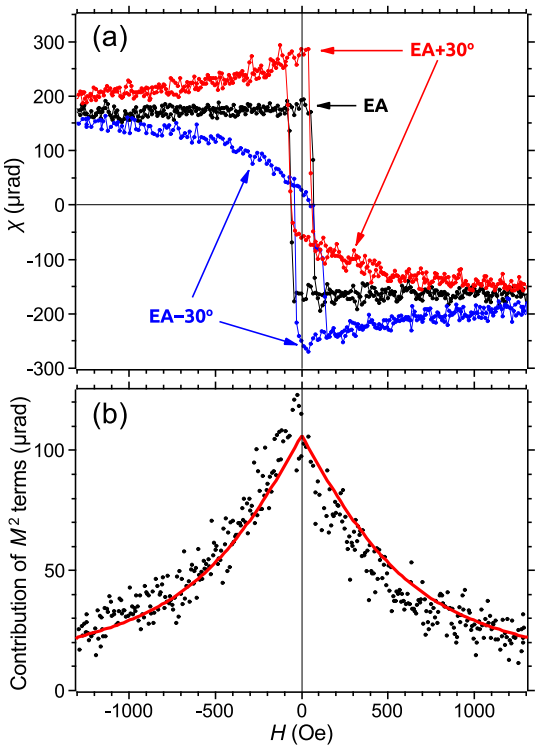

FIG. 10. (a) Magnetic field dependence of angle χ charactering the ellipticity of light reflected from CoFeB layer in LMOKE geometry for orientation of magnetic field along EA and at angles $\psi = 30^\circ$ (EA + 30°) and $\psi = -30^\circ$ (EA-30°). (b) The half difference of hysteresis curves $\Delta\chi$ (H) (dots) and calculated $M_u(H)$ $M_v(H)$ (solid line). The value of the parameter $k_{c1} = K_{c1}/M_s$ was taken from Eq. (5).

deviation of the applied field from the normal to the film plane or by its inhomogeneity within the sample.

The presence of in-plane biaxial magnetic anisotropy is also confirmed by magneto-optical hysteresis loops measured by LMOKE. The shape of LMOKE hysteresis loops strongly depend on the orientation of magnetic field relative to crystal axes. For orientation of magnetic field along [110], which is the easy magnetization axis (EA), the hysteresis loops [Fig. 10(a), black line] have square shape and are antisymmetric in (H, χ) coordinates, where χ is the angle characterizing the reflected light ellipticity. It is seen that χ (H) is constant, except for the points $H = \pm H_c$, where the magnetization jumps and χ (H) changes steeply. For other magnetic field azimuths (red and blue lines), apart from the points $H = \pm H_c$, there are gradual slopes in χ (H) due to magnetization rotation. The shape of these slopes depends on the angle ψ between magnetic field and the easy axis and reveals 90° periodicity.

Analogous LMOKE behavior has been observed earlier in Fe/Cr/GaAs(001) heterostructures and was attributed to manifestation of quadratic in magnetization terms proportional to $M_u M_v$ [38], where M_u is the projection of **M** onto direction of **H**, M_v—perpendicular to it in the film plane (see inset in Fig. 5). At optical frequencies, the terms in the dielectric tensor, quadratic in magnetization components, result in a change of magnetic layer optical indicatrix, which depends on the

in-plane orientation of magnetization. Manifestation of these terms in the case of in-plane uniaxial magnetic anisotropy has been observed also in Co films grown on corrugated CaF_2/Si structures [39].

Experimentally, the contribution $\Delta\chi\ (H)$ of quadratic in magnetization terms can be obtained [37] by taking the difference of LMOKE magnetic field dependencies for two magnetic field orientations: at angles $+\psi$ and $-\psi$ relative to EA [Fig. 10(b), dots]. It should match the product $M_u(H)M_v(H)$ that is calculated within the minimization procedure (Sec. IV A) and with the same parameters as found by FMR and VSM studies:

$$\Delta\chi(H) = \left|\frac{\chi(H,+\psi) - \chi(H,-\psi)}{2}\right| \propto |M_u(H)M_v(H)|. \tag{7}$$

It is important to note, that being normalized by its magnitude at $H = 0$ the $M_u(H)\ M_v(H)$ curve [Fig. 10(b), red line] depends on ψ and on a single parameter $k_{c1} = K_{c1}/M_s$. The latter could be determined from the wings of $\Delta\chi\ (H)$, although with less accuracy than that obtained from FMR.

V. CONCLUSIONS

The study carried out in this work shows that the epitaxial CoFeB films can be grown on MgO (001) and (111) surfaces by laser MBE technique using single stage regime with high growth temperature. Crystal structure and magnetic parameters of films fabricated by this technique considerably differ from those prepared by usual two stage method when at the first stage the amorphous films are grown at room temperature and at second stage high-temperature annealing is used for the crystallization of the film. In contrast to the textured bcc or polycrystalline films obtained by the growth-plus-annealing technique in earlier studies the high-temperature CoFeB/MgO films fabricated in the present work are epitaxial and have bcc structure as proved by XRD and RHEED studies. As it is well known, the epitaxial growth of layers using laser molecular beam is a very nonequilibrium process. It is strongly different from much closer to the equilibrium annealing procedure, the influence of which on the properties of CoFeB/MgO heterostructures has been recently studied in detail in Ref. [13]. This can result in dissimilar boron distribution in films grown by different methods and may be the reason why CoFeB epitaxial, likely metastable, films appear in our experiments. When grown on MgO(001) surface the CoFeB crystallites are oriented in the same way showing the following epitaxial relations: CoFeB [001] ‖ MgO [001], CoFeB [010] ‖ MgO [110]. In the CoFeB/MgO(111) system a three-domain growth was observed with nontrivial epitaxial relations: CoFeB [110] ‖ MgO [111], CoFeB[001] ‖ MgO$\langle -110\rangle$. Interestingly, the $[\sqrt{2}\times\sqrt{2}R45]$ superstructure was observed on CoFeB(001) surface; its possible explanation was suggested.

The differences in crystalline properties of films prepared by one- and two-stage techniques manifest itself in their magnetic properties. The CoFeB/MgO(001) structures grown in this work clearly reveal the in-plane biaxial magnetic anisotropy without any admixture of uniaxial anisotropy which is usually observed in films prepared by the two step technique. Depending on orientation of in-plane magnetic field the in-plane magnetization reversal process in the studied films is accompanied by magnetization rotation and one or two nonreversible jumps. Magnetization jumps occur though nucleation and movement of domain walls and correspond to transition into metastable or stable states. Note that magnetic and magneto-optical properties of the studied CoFeB films are quite similar to those of well-known model Fe/Cr/GaAs(001) heterostructures [40]. Minimal FMR line width $\Delta H \sim 35$ Oe is close to the smallest ΔH values observed in the metallic films (see, e.g., Refs. [30] and [31]). The approach adopted in this work enables fabrication of a number of heterostructures attractive for spintronic applications.

ACKNOWLEGMENTS

The XRD measurements have been carried out at BL3A beamline of Photon Factory synchrotron (Tsukuba, Japan) along the proposal 2016G684. The work has been supported by Russian Foundation for Basic Research (Grant No. 17-02-00729). FMR measurements have been supported by the Government of the Russian Federation via project No.14.Z50.31.0021 in P220 Program. XRD characterization was partly carried out using equipment of the Joint Research Center "Material science and characterization in advanced technology" (Ioffe Institute, St. Petersburg, Russia).

[1] L. Bainsla, K. G. Suresh, A. K. Nigam, M. M. Raja, B. S. D. Ch. S. Varaprasad, Y. K. Takahashi, and K. Hono, High spin polarization in CoFeMnGe equiatomic quaternary Heusler alloy, J. Appl. Phys. **116**, 203902 (2014).

[2] A. McNichol Boldin, Analysis of Spin Polarization in Half-Metallic Heusler Alloys, Macalester J. Phys. Astron. **3**, 3 (2015).

[3] S. Parkin, C. Kaiser, A. Panchula, P. Rice, B. Hughes, M. Samant, and See-Hun Yang, Giant tunnelling magnetoresistance at room temperature with MgO (100) tunnel barriers, Nat. Mater. **3**, 862 (2004).

[4] J. Fabian, A. Matos-Abiaguea, C. Ertlera, P. Stano, and I. Zuti, Semiconductor spintronics, Acta Phys. Slovaca **57**, 565 (2007).

[5] J. F. Gregg, R. P. Borges, E. Jouguelet, C. L. Dennis, I. Petej, S. M. Thompson, and K. Ounadjela, Spin injection efficiency in spin electronic devices, J. Magn. Magn. Mater. **265**, 274 (2003).

[6] A. Conca, J. Greser, T. Sebastian, S. Klingler, B. Obry, B. Leven, and B. Hillebrands, Low spin-wave damping in amorphous $Co_{40}Fe_{40}B_{20}$ thin films, J. Appl. Phys. **113**, 213909 (2013).

[7] S. Ikeda, J. Hayakawa, Y. M. Lee, T. Tanikawa, F. Matsukura, and H. Ohno, Tunnel magnetoresistance in MgO-barrier magnetic tunnel junctions with bcc-CoFe(B) and fcc-CoFe free layers, J. Appl. Phys. **99**, 08A907 (2006).

[8] G. Viaud and N. A. Pertsev, Dynamic converse magnetoelectric effect in ferromagnetic nanostructures with electric-field-dependent interfacial anisotropy, Phys. Rev. B **90**, 064429 (2014).

[9] S. Rizwan, G. Q. Yu, S. Zhang, Y. G. Zhao, and X. F. Han, Electric-field control of CoFeB/IrMn exchange bias system, J. Appl. Phys. **112**, 064120 (2012).

[10] Xu Zhang, Y. Zhang, and J. W. Cai, Large Perpendicular Exchange Bias in CoFeB/MgO Systems Pinned by a Bottom

IrMn Layer via an Interfacial CoFe/Ta Composite Layer, IEEE Trans. Magn. **51**, 4800604 (2015).

[11] M. Munakata, Shin-Ichi Aoqui, and M. Yagi, Low spin-wave damping in amorphous $Co_{40}Fe_{40}B_{20}$ thin films, IEEE Trans. Magn. **41**, 3262 (2005).

[12] V. Harnchana, A. T. Hindmarch, M. C. Sarahan, C. H. Marrows, A. P. Brown, and R. M. D. Brydson, Evidence for boron diffusion into sub-stoichiometric MgO (001) barriers in CoFeB/MgO-based magnetic tunnel junctions, J. Appl. Phys. **113**, 163502 (2013).

[13] S. Mukherjee, R. Knut, S. M. Mohseni *et al.*, Role of boron diffusion in CoFeB/MgO magnetic tunnel junctions, Phys. Rev. B **91**, 085311 (2015).

[14] A. Verma, B. Ghosh, B. Awadhiya, and T. Kumar, *AbInitio* Modeling of Effect of Boron and Phosphorus Doping in CoFe/MgO Magnetic Tunnel Junctions, J. Low Power Electr. **10**, 361 (2014).

[15] W. Butler, Tunneling magnetoresistance from a symmetry filtering effect, Sci. Technol. Adv. Mater. **9**, 014106 (2008).

[16] J. Y. Bae, W. C. Lim, H. J. Kim, T. D. Lee, K. W. Kim, and T. W. Kim, Compositional change of MgO barrier and interface in CoFeB/MgO/CoFeBCoFeB/MgO/CoFeB tunnel junction after annealing, J. Appl. Phys. **99**, 08T316 (2006).

[17] S. Yuasa, Y. Suzuki, T. Katayama, and K. Ando, Characterization of growth and crystallization processes in CoFeB/MgO/CoFeBCoFeB/MgO/CoFeB magnetic tunnel junction structure by reflective high-energy electron diffraction, Appl. Phys. Lett. **87**, 242503 (2005).

[18] S. M. Suturin, V. V. Fedorov, A. M. Korovin, G. A. Valkovskiy, S. G. Konnikov, M. Tabuchi, and N. S. Sokolov, A look inside epitaxial cobalt-on-fluorite nanoparticles with three-dimensional reciprocal space mapping using GIXD, RHEED and GISAXS, J. Appl. Cryst. **46**, 874 (2013).

[19] S. M. Suturin, A. M. Korovin, V. V. Fedorov, G. A. Valkovsky, M. Tabuchi, and N. S. Sokolov, An advanced three-dimensional RHEED mapping approach to the diffraction study of Co/MnF2/CaF2/Si(001) epitaxial heterostructures, J. Appl. Cryst. **49**, 1532 (2016).

[20] N. S. Sokolov, V. V Fedorov, A. M. Korovin, S. M. Suturin, D. A. Baranov, S. V. Gastev, B. B. Krichevtsov, K. Y. Maksimova, A. I. Grunin, V. E. Bursian, L. V. Lutsev, and M. Tabuchi, Thin yttrium iron garnet films grown by pulsed laser deposition: Crystal structure, static, and dynamic magnetic properties, J. Appl. Phys. **119**, 023903 (2016).

[21] B. B. Krichevtsov, S. V. Gastev, S. M. Suturin, V. V. Fedorov, A. M. Korovin, V. E. Bursian, A. G. Banshchikov, M. P. Volkov, M. Tabuchi, and N. S. Sokolov, Magnetization reversal in YIG/GGG(111) nanoheterostructures grown by laser molecular beam epitaxy, Sci. Technol. Adv. Mater. **18**, 351 (2017).

[22] T. Takeuchi, K. Tsunekava, Young-suk Choi, Yoshinori Nagamine, D. D. Djayaprawira, A. Gensek, Y. Hoshi, and Y. Kitamoto, Crystallization of Amorphous CoFeB Ferromagnetic Layers in CoFeB/MgO/CoFeB Magnetic Tunnel Junctions, Jpn. J. Appl. Phys. **46**, L623 (2007).

[23] K. H. J. Buschow, P. G. van Engen, and R. Jongebreur, Magneto-optical properties of metallic ferromagnetic materials, J. Magn. Magn. Mater. **38**, 1 (1983).

[24] A. G. Banshchikov, S. V. Gastev, A. K. Kaveev, B. B. Krichevtsov, Yu. Yu. Petrova, S. M. Suturin, V. P. Ulin, M. P. Volkov, and N. S. Sokolov, Characterization of epitaxial $Co_{40}Fe_{40}B_{20}$ magnetic thin films grown on GaAs(001), in *Proceedings of the 24th International Symposium on Nanostructures: Physics and Technology, St. Petersburg June 27–July 1, 2016* (St. Petersburg Academic University, St. Petersburg, 2016), p. 262.

[25] I. Khan and J. Hong, Magnetic anisotropy of C and N doped bulk FeCo alloy: A first principles study, J. Magn. Magn. Mater. **388**, 101 (2015).

[26] D. M. Forrester, F. V. Kusmartsev, and E. Kovács, Designing magnetic superlattices that are composed of single domain nanomagnets, Beilstein J. Nanotechnol. **5**, 956 (2014).

[27] Xuan-Zhang Wang, Quan Liu, Shu-Chang Wang, and Yan Zhao, Magnetic properties of antiferromagnetic superlattices, J. Phys.: Condens. Matter **5**, 3443 (1993).

[28] H. S. Craft, J. F. Ihlefeld, M. D. Losego, R. Collazo, Z. Sitar, and J-P. Maria, MgO epitaxy on GaN (0002) surfaces by molecular beam epitaxy, Appl. Phys. Lett. **88**, 212906 (2006).

[29] M. Losego, Interfacing Epitaxial Oxides to Gallium Nitride, Ph.D. Thesis, Materials Science and Engineering, Raleigh, North Carolina 2008.

[30] X. Liu, W. Zhang, M. J. Carter, and G. Xiao, Ferromagnetic resonance and damping properties of CoFeB thin films as free layers in MgO-based magnetic tunnel junctions, J. Appl. Phys. **110**, 033910 (2011).

[31] G. V. Swamy, R. K. Rakshit, R. P. Pant, and G. A. Basheed, Origin of "in-plane" and "out-of-plane" magnetic anisotropies in as-deposited and annealed CoFeB ferromagnetic thin films, J. Appl. Phys. **117**, 17A312 (2015).

[32] B. Heinrich. Ferromagnetic resonance in ultrathin film structures. In *Ultrathin Magnetic Structures II,* edited by B. Heinrich and J. A. C. Bland (Springer-Verlag, Berlin/Heidelberg,1994).

[33] H. X. Yang, M. Chshiev, B. Dieny, J. H. Lee, A. Manchon, and K. H. Shin, First-principles investigation of the very large perpendicular magnetic anisotropy at Fe/MgO and Co/MgO interfaces, Phys. Rev. B **84**, 054401 (2011).

[34] S. Iihama, S. Mizukami, H. Naganuma, M. Oogane, Y. Ando, and T. Miyazaki, Gilbert damping constants of Ta/CoFeB/MgO(Ta) thin films measured by optical detection of precessional magnetization dynamics, Phys. Rev. B **89**, 174416 (2014).

[35] C. J. Gutierrez, G. A. Prinz, J. J. Krebs, M. E. Filihkowski, V. G. Harris, and W. T. Elam, Magnetic and structural studies of epitaxial (001) Fe and (001) $Fe_xCo_{(1-x)}$ alloy film structures, J. Magn. Magn. Mater. **126**, 232 (1993).

[36] Z. Miao-Ling, J. Ye, R. Liu, Sh. Mi, Y. Xie, Hao-ling Liu, C. Van Haesendonck, and Zi-Yu Chen, Study of magnetization reversal and anisotropy of single crystalline ultrathin Fe/MgO (001) film by magneto-optic Kerr effect, Chin. Phys. B **25**, 047503 (2016).

[37] V. B. Naik, H. Meng, and R. Sbiaa, Thick CoFeB with perpendicular magnetic anisotropy in CoFeB-MgO based magnetic tunnel junction, AIP Adv. **2**, 042182 (2012).

[38] A. A. Rzhevsky, B. B. Krichevtsov, D. E. Bürgler, and C. M. Schneider, Magnetization dynamics induced by ultrashort optical pulses in Fe/Cr thin films, Phys. Rev. B **75**, 224434 (2007).

[39] B. B. Krichevtsov, A. K. Kaveev, A. Balanev, N. S. Sokolov, J. Camarero, and R. Miranda, Magnetic and magneto-optical properties of epitaxial cobalt films grown on a corrugated CaF2/Si surface, Phys. Solid State **49**, 1481 (2007).

[40] B. Heinrich and J. F. Cochran, Ultrathin metallic magnetic films: Magnetic anisotropies and exchange interactions, Adv. Phys. **42**, 523 (1993).